Prabha Materials Science Letters
Vol. 5, No. 2, 502-519, 2026
https://doi.org/10.33889/PMSL.2026.5.2.027

Improvement in Power Conversion Efficiency of Perovskite Solar Cell by Introducing SnO_2 as an Electron Transport Layer: A Numerical Simulation Study

Yogmaya Sharma
Department of Sciences (Physics),
Manav Rachna University, Aravalli Hills, 121004, Faridabad, Haryana, India.
E-mail: sharmayogita1985@gmail.com
ORCID: https://orcid.org/0000-0002-9511-2915

Anshuman Sahai
Department of Sciences (Physics),
Manav Rachna University, Aravalli Hills, 121004, Faridabad, Haryana, India.
E-mail: anshuman@mru.edu.in
ORCID: https://orcid.org/0000-0003-4112-6120

Shiv Kumar Dixit
Department of Electronics and Communication Engineering,
School of Engineering, Manav Rachna University, 121004, Faridabad, Haryana, India.
Corresponding author: shivkumardixit.7@gmail.com
ORCID: https://orcid.org/0009-0000-9386-4606

Chhavi Bhatnagar
Maharaja Agrasen College,
University of Delhi, 110096, Delhi, India.
E-mail: chhavijp90@gmail.com
ORCID: https://orcid.org/0009-0001-9098-9793

(Received on December 31, 2025; Revised on May 10, 2026 & July 18, 2026; Accepted on August 8, 2026)

Abstract
Solar cells consisting of perovskites materials have shown great interest because of their low cost and high-power conversion efficiency (PCE). But still there are some issues such as limited absorption, hysteresis and device instability. In the present work we have simulated the formamidinium lead tri-iodide ($FAPbI_3$) based perovskite solar cell and the effect of incorporation of SnO_2 Electron transport layer (ETL) on the power conversion efficiency of solar cell has been investigated. The device without SnO_2 layer shows low efficiency of 21.71 % at 267 Kelvin. But after incorporation of ETL, the device obtained a PCE of 24 % at 267 Kelvin. The effect of thickness of hole transport layer (HTL), ETL and doping density on the PCE has been analysed using Solar cell capacitance simulator (SCAPS-1D) software tool. This study shows that $FAPbI_3$ may be a promising material for enhancing the PCE of perovskite solar cells (PSCs).

Keywords- SnO_2, SCAPS-1D, PCE, Perovskite solar cells, Numerical simulation.

1. Introduction

Every day, the mother earth receives an immense amount of solar energy, making sunlight as one of the most abundant and sustainable energy sources. Solar energy is very economical, renewable and also available in abundant and it can be stored in large storage system like batteries, artificial dams etc (Xie et al., 2023), but there is lot of scope for further development and improvement in material science and the

research is going on all over the world to increase the efficiency of conversion by 30-40% (Chen et al., 2018; Hosen et al., 2023; ElKhamisy et al., 2024; Sikder et al., 2024; Uddin et al., 2024). At present silicon based solar cells are being used that have achieved 25% of PCE and are commercialised at large scale (Andreani et al., 2019). However, silicon-based solar cells suffer from several limitations, including strong dependence on operating conditions, bulky module size, high installation cost and of course lot of carbon emission (pollution) during purification of silicon. These challenges have motivated researchers to tackle problems on next-generation photovoltaic technologies (Kojima et al., 2009).

First generation solar cells were discovered in 1954 by Bell Labs for commercial production, but due to high cost and rigidity (Chen et al., 2022) these were failed and other type of second generation solar cells were developed. The main challenge with second generation cells was lower efficiency, and shorter life span (Tsarev et al., 2023). Hence to overcome all these problems, third-generation solar cells especially perovskite solar cells (PSCs) have emerged as an alternative to first and second generation cells. The first report on PSCs demonstrated a modest PCE of 3.8%; however, rapid advancements have increased efficiencies to over 20.5% within ten years (Yin et al., 2014; Bertoluzzi & Bisquert, 2017; Ravishankar et al., 2019; Gabriela et al., 2022). Perovskite materials, characterized by the ABX_3 crystal structure, offer several advantages such as low-cost fabrication, lightweight architecture, excellent compatibility with flexible substrates, and outstanding optoelectronic properties like high absorption coefficients, tunable bandgap, long charge carriers diffusion length and high charge carriers mobility (Guerrero et al., 2021; Hernández-Balaguera & Bisquert, 2022; Huo et al., 2022; Xia et al., 2022). In PSCs devices, the perovskite layer acts as the light absorber, where photon absorption generates electron hole pairs that are selectively extracted by the electron transport layer (ETL) and hole transport layer (HTL), respectively (Liu et al., 2017). However, simulation studies have provided the better insight about the system as a whole without wasting any resource and time. To optimise the performance while reducing fabrication cost and time, solar cell modelling and simulation tools have gained significant importance.

There are many simulation software available in market like PVsyst, Aurora Solar, Silvaco Atlas and Solar Capacitance Simulator (SCAPS-1D). We have used SCAPS-1D software as it is a open source and capability of driving different parameters like electrical simulation, material and layer definition, defect modelling, temperature and illumination control. It has simplest interface & no programming is required. In recent years, one-dimensional solar cell simulation software such as SCAPS-1D has been extensively employed to analyse charge transport, recombination mechanisms, and overall solar cell performance in various photovoltaic architectures (Salgado-Conrado et al., 2024). Efficient charge extraction and transport are critical for enhancing PSCs performance. The photogenerated charge carriers must be transported to the electrodes with minimal losses. Therefore, the selection of suitable charge transport layer (CTL) plays a decisive role in determining solar cell efficiency and stability (Schulz, 2018). Other organic CTLs such as PEDOT: PSS, P3HT, and spiro-OMeTAD offer advantages including low-temperature solution processing and mechanical flexibility. However, their practical application is limited by chemical instability, low charge carrier mobility, and high production costs (Yoo et al., 2019). In contrast, inorganic metal oxide-based CTLs have attracted considerable attention due to their low cost, controlled synthesis, high carrier mobility, excellent chemical stability, and tuneable optoelectronic properties (Mahapatra & Lee, 2022). The use of metal oxide ETLs and HTLs has been shown to significantly enhance both PCE and Solar Cell stability, while also suppressing perovskite degradation at the interfaces (Kim et al., 2012; Wang & Kumar, 2022; Wang et al., 2022a; Wang et al., 2022b). Hybrid perovskite solar cells exhibit remarkable properties such as wide band gaps, high absorption coefficients, low exciton binding energies, reduced surface recombination, high charge carrier mobility, and long diffusion lengths, enabling power conversion efficiencies exceeding 25%. These attributes position PSCs among the most promising photovoltaic technologies available today. Since the pioneering work by

Kojima in 2009 using iodide- and bromide-based perovskites, which achieved a PCE of 3.81%, significant milestones have been reached. The efficiency increased to 6.54% in 2011, 16.2% in 2013, and 19.3% following TiO_2 layer optimization (Kojima et al., 2009). Subsequent advancements led to efficiencies exceeding 20% by 2017, and 23% by 2019 using methylammonium lead triiodide ($MAPbI_3$). Despite these achievements, PSC efficiencies remain below the Shockley–Queisser theoretical limit of approximately 31.4% (Shockley & Queisser, 1961). Although $MAPbI_3$-based PSCs have demonstrated high efficiency, concerns regarding moisture sensitivity and long-term stability persist (Moyez & Roy, 2018; Jamal et al., 2019; Jena et al., 2019; Rai et al., 2020; Kanoun et al., 2021). Formamidinium lead triiodide ($FAPbI_3$) has emerged as a more thermally stable alternative, with a favourable band gap of 1.51 eV that enables improved solar spectrum absorption (Eperon et al., 2014; Wozny et al., 2015; Han et al., 2016; Pandey & Chaujar, 2017; Wang et al., 2024).

Hossain et al. (2025) have recently used $FAPbI_3$ as an absorbing layer with Spiro-OMeTAD as HTL and sulfur-doped tin oxide (STO) as the ETL and simulated the structure using SCAPS-1D and obtained a PCE of 22.58 %. Chen et al. (2024) have used alpha phase $FAPbI_3$ with Spiro-OMeTAD and SnO_2 as HTL and ETL respectively and obtained a PCE of 22.4% experimentally.

Among HTLs, spiro-OMeTAD is widely used; however, its reliance on additives such as Li-TFSI (Lithium bis (trifluoromethanesulfonyl)imide) and TBP (4-tert-Butylpyridine) introduces stability issues, including perovskite degradation and increased solar cell corrosion (Wang et al., 2016). Similarly, PEDOT: PSS suffers from acidic corrosion and limited durability. These limitations have driven the search for efficient, stable, and low-cost inorganic HTL alternatives (Haider et al., 2018). On the electron transport side, numerous n-type metal oxides including TiO_2, ZnO, Zn_2SnO_4, WO_3, In_2O_3, $SrTiO_3$, Nb_2O_5, CeO_x, SnO_2, and $BaSnO_3$ (Kim et al., 2013; Hao et al., 2014; Son et al., 2014; Chen et al., 2017; Yang et al., 2017; National Renewable Energy Laboratory, 2018; Ishchenko et al., 2021) have been explored and among them TiO_2 despite widely used suffers from low electron mobility, UV-induced instability, and the need of high-temperature processing. ZnO enables low-temperature fabrication but exhibits surface hydroxyl groups that degrade perovskite layers.

Among these materials, SnO_2 has emerged as a highly promising ETL due to its superior optical transparency, favourable band alignment, high electron mobility, reduced UV absorption, low hygroscopicity, and excellent chemical stability (Jiang et al., 2017). Additionally, low-temperature-processed SnO_2 offers cost-effective fabrication and enhanced Solar Cell longevity, making it an ideal candidate for high-performance and stable perovskite solar cells. The high electron mobility, high optical transmittance, low temperature processing capability, and appropriate energy level alignment with perovskite absorber, Tin Oxide (SnO_2) has emerged as a promising material for PV technology (Xiong et al., 2018).

In the present work, we have explored the $FAPbI_3$ layer by varying absorber layer thickness, temperature and doping concentration in the device with and without SnO_2 ETL and parameters are optimized for better power conversion efficiency.

2. Device Structure and Simulation

The solar cell capacitance simulator software SCAPS (Ver.3.3.10) under solar spectrum AM1.5G ($100 mW/cm^2$) at 300 K has been used to measure output parameters of the perovskite solar cell. It is a 1D optoelectrical simulator tool which can simulate 7 layers at a time. The working principle of SCAPS-1D is based on Continuity & Poisson equations (Minemoto & Murata, 2014; Abdelaziz et al., 2019). The simulated p-i-n structure is composed of $FTO/NiO_x/FAPbI_3/C_{60}/SnO_2/Au$ material layers.

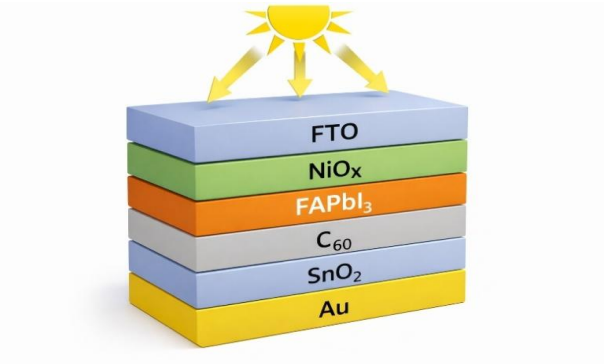

Figure 1. Schematic of $FAPbI_3$ based PSC structure used for simulation.

The structure of the PSC employed in the initial simulation process as illustrated (**Figure 1**), which comprise of FTO-Coated glass, NiO_x as hole transport layer (HTL), $FAPbI_3$ as light absorbing material, C_{60} and SnO_2 both as electron transport layer (ETL) and Au for the electrode. The basic material properties are extracted from various theoretical and experimental results which are listed in **Table 1**. The work function of FTO and back electrode Au is taken as 4.04 eV and 5.9 eV respectively (Noman et al., 2023).

Table 1. Physical properties of materials used in initial simulations.

Material properties	**FTO**	**NiO_X**	**$FAPbI_3$**	**C_{60}**	**SnO_2**
Thickness (nm)	500	80	550	50	100
Band gap (eV)	3.2	3.75	1.51	1.7	3.6
e^- affinity (eV)	4.4	2.1	4	3.9	4
Permittivity	9	10.7	6.6	4.2	9
CB effective density of state (cm^{-3})	2×10^{18}	2.80×10^{19}	1.20×10^{19}	8×10^{19}	2.20×10^{18}
VB effective density of state (cm^{-3})	1.8×10^{19}	1.80×10^{19}	2.9×10^{13}	8×10^{19}	1.80×10^{19}
Mobility of electron (μ_e) cm^2/Vs	20	12	2.7	$8 X 10^{-2}$	240
Mobility of holes (μ_h) cm^2/Vs	1×10^6	2.8	1.8	3.5×10^{-3}	220
Density of n-type doping	10^{13}	0	$1.90 X 10^{15}$	1×10^{17}	1×10^{19}
Density of p-type doping	-	1×10^{15}	$1.90 X 10^{15}$	0	0
Density of defects	10^8	1×10^{15}	$1 X 10^{15}$	$1 X 10^{15}$	$1 X 10^{15}$
References	Azadinia et al. (2021), Raj et al. (2021)	Haider et al. (2018)	Noman et al. (2023)	Noman et al. (2023)	Fatima et al. (2023)

3. Results and Discussion

The primary focus of this work is to investigate the effect of ETL on the performance of $FAPbI_3$ solar cell. In this regard, the thickness of absorber, ETL and HTL layer is varied and optimized. The device is also simulated under the effect of temperature from 267 Kelvin to 400 Kelvin and results are optimized.

From **Figure 2**, the higher value of (a) JV and (b) EQE shows that role of SnO_2 ETL in the device is significant. The device with SnO_2 ETL achieved a PCE of 22.27% and EQE of more than 98% at lower wavelength region (300-600nm) while the device without SnO_2 ETL obtained a PCE of 20.22% and EQE of 78%. At lower wavelength region without SnO_2 ETL the EQE decreases due to more front surface recombination and thermalization losses. After incorporation of SnO_2 ETL, ultrafast charge transfer is taking place and JV and EQE both are increased. However, researchers have used other perovskites also

with SnO_2 ETL. Jiang et al. (2017) have used SnO_2 ETL with $HC(NH_2)$ PbI_3 based perovskite solar cell and reported a PCE of 19.9%.

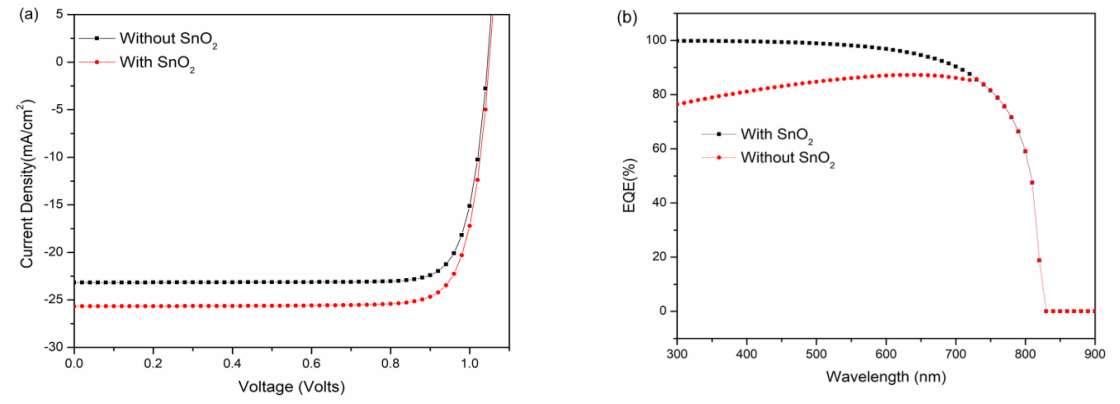

Figure 2. Comparison of (a) JV characteristics and (b) EQE for the devices with and without SnO_2 ETL.

3.1 Effect of Absorber Layer Thickness

The perovskite layer which generates charge carriers by absorbing light is critical to solar cell performance. The photovoltaic properties of PSCs are greatly influenced by absorber thickness. The absorber layer thickness determines its quality such as film morphology, which directly influences photogenerated carrier lifetime and diffusion length. To study the significance of absorber layer thickness on PSC performance, the thickness was varied from 200nm-1200nm.

The variation of photovoltaic parameter with thickness of absorber layer is illustrated in the **Figure 3**. It can be seen that as we start increasing the thickness, the short circuit current density (J_{sc}) of the cell with and without SnO_2 electron transport layer (ETL) increases and both the curves exhibit same trend (**Figure 3(a)**). Solar cell with SnO_2 reaches a maximum J_{sc} of 27.5 mA/cm^2 compared to without SnO_2 of 25.08mA/cm^2. The gap between the two curves widens at lower thicknesses and remains significant as thickness increases. The increase in short-circuit current density J_{sc} for the SnO_2 based device can be attributed to more efficient photogenerated electron collection at the perovskite/electron transport layer interface. The conduction band position of SnO_2 is well aligned with that of the perovskite absorber, which promotes rapid electron transfer while simultaneously acting as a barrier to hole backflow, thereby limiting interfacial recombination. Furthermore, the relatively high electron mobility and low density of trap states in SnO_2 support improved carrier transport toward the electrode. The effect becomes particularly significant in thinner absorber layers, where recombination losses are more dominant, making efficient interfacial charge extraction essential for sustaining higher photocurrent.

The **Figure 3(b)** illustrates that the open-circuit voltage (V_{oc}) depends on absorber thickness. At small thicknesses (around 250–300nm), both architectures deliver their highest V_{oc} values, close to 1.10 V, and the SnO_2-based solar cell shows a slight but systematic voltage enhancement relative to the one without SnO_2. As the thickness is increased up to 1200 nm, V_{oc} steadily declines for both structures by several tens of millivolts, yet the SnO_2 solar cell consistently retains a small voltage lead across the entire range. Thicker absorber layers increase the path length for carrier transport and expose carriers to more bulk defects, which strengthens non-radiative recombination and reduces the quasi-Fermi-level splitting, leading to the observed drop in V_{oc} with thickness. The persistent voltage gain in the presence of SnO_2

implies that this layer improves electron extraction and suppresses interfacial recombination—likely through more favourable band alignment or partial passivation of interface traps—so that the negative impact of thickness-induced recombination is somewhat mitigated.

The **Figure 3(c)** shows that fill factor (FF) decreases with increasing absorber thickness for both solar cell types, and that solar cell with the SnO_2 layer exhibit a stronger degradation in FF at larger thicknesses than solar cell without SnO_2. At low thickness (200-400 nm), both solar cells reach similar maximum FF values around 83–84%, indicating that when the absorber is relatively thin, series resistance and recombination are comparatively low and the influence of SnO_2 on FF is minimal. As thickness increases beyond 400 nm, the FF of the SnO_2-containing Solar Cell drops more steeply (from 83% to 77% at 1200 nm), whereas the FF of the solar cell without SnO_2 decreases slightly (staying above 82%). Increasing thickness enhances optical absorption but also increases bulk and interfacial recombination due to longer carrier transport paths and possible defect accumulation in the perovskite bulk. This leads to higher series resistance and lower FF for both the architectures. The effect of $FAPbI_3$ absorber layer thickness on output parameters is given in **Table 2**.

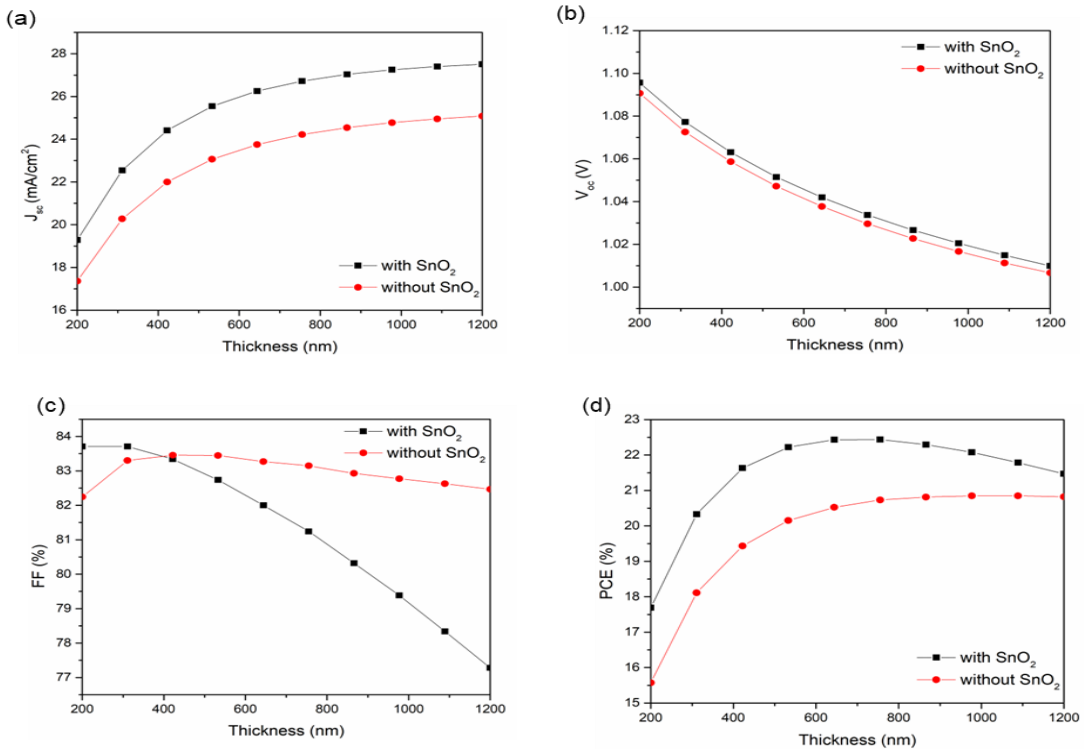

Figure 3. Variation of (a) J_{sc}, (b) V_{OC}, (c) FF and (d) PCE with the change of absorber layer thickness.

Table 2. Effect of $FAPbI_3$ absorber thickness variation on output parameters.

Device structure	Thickness (nm)	V_{oc} (V)	J_{sc} (mA/cm^2)	FF (%)	PCE (%)
With SnO_2	200	1.10	19.29	83.71	17.69
Without SnO_2		1.09	17.36	82.24	15.57
With SnO_2	311	1.08	22.54	83.71	20.33
Without SnO_2		1.07	20.27	83.30	18.11

Table 2 continued…

With SnO_2	422	1.06	24.42	83.34	21.63
Without SnO_2		1.06	22.00	83.45	19.43
With SnO_2	533	1.05	25.54	82.74	22.22
Without SnO_2		1.05	23.06	83.45	20.15
With SnO_2	644	1.04	26.25	82.00	22.43
Without SnO_2		1.04	23.75	83.27	20.52
With SnO_2	755	1.03	26.72	81.24	22.44
Without SnO_2		1.03	24.22	83.15	20.73
With SnO_2	866	1.03	27.03	80.32	22.29
Without SnO_2		1.02	24.54	82.93	20.81
With SnO_2	977	1.02	27.25	79.38	22.08
Without SnO_2		1.02	24.78	82.77	20.85
With SnO_2	1089	1.01	27.40	78.34	21.79
Without SnO_2		1.01	24.95	82.63	20.85
With SnO_2	1200	1.01	27.51	77.28	21.47
Without SnO_2		1.01	25.08	82.47	20.82

3.2 Effect of Temperature on the Device

The temperature-dependent photovoltaic parameters of the perovskite solar cell, with and without the incorporation of SnO_2 interfacial layer, are presented in **Figure 4 (a-d)**. As shown in **Figure 4(a)**, the short-circuit current density (J_{sc}) remains nearly temperature-independent for both devices, indicating stable photogeneration across the investigated temperature range. Notably, the device incorporating SnO_2 consistently exhibits a higher J_{sc}, attributed to improved electron extraction and reduced interfacial recombination losses at the ETL/perovskite interface. As the temperature (T) increases Voc is mostly affected and the relation of temperature and Voc is given in Equation (1).

$$Voc(T) = \frac{\eta K_B T}{q} \ln\left(\frac{J_{ph}}{J_o(T)} + 1\right) \quad (1)$$

Temperature dependent saturation current (J_o) also rises exponentially with T and Voc decreases but the effect of temperature on Jsc is very less as shown in **Figure 4(a)** and can be seen from the Equation (2) also. When the temperature increases, bandgap decreases and photons having less energy contribute in generation of e-h pairs but this effect is very small and J_{sc} is mostly independent on temperature.

$$J_{sc}(T) = J_{sc}(T_{ref})\,[1+ \mu_{1sc}(T-T_{ref})] \quad (2)$$

where, μ_{1sc} is temperature coefficient of short circuit current (Pindado & Cubas, 2017; Honsberg & Bowden, 2019).

Figure 4(b) illustrates a monotonic decrease in open-circuit voltage (V_{oc}) with increasing temperature, consistent with enhanced non-radiative recombination and reduced quasi-Fermi level splitting at elevated temperatures. The SnO_2 based device maintains a slightly higher V_{oc} across the entire temperature range, reflecting effective suppression of recombination and improved band alignment.

As depicted in **Figure 4(c)**, the fill factor (FF) decreases with temperature due to increased carrier scattering and series resistance. However, the device without SnO_2 shows marginally higher FF values, which may be associated with differences in interfacial resistance or charge transport balance under thermal stress. Consequently, the power conversion efficiency (PCE) as shown in **Figure 4(d)** declines with increasing temperature for both configurations, driven primarily by reductions in V_{oc} and FF. Despite this trend, the SnO_2 based device consistently delivers higher PCE, demonstrating superior thermal stability and highlighting the critical role of SnO_2 in enhancing charge extraction and mitigating

temperature-induced performance degradation. The data on effect of temperature on solar cell output parameters with and without SnO_2 ETL is given in **Table 3**.

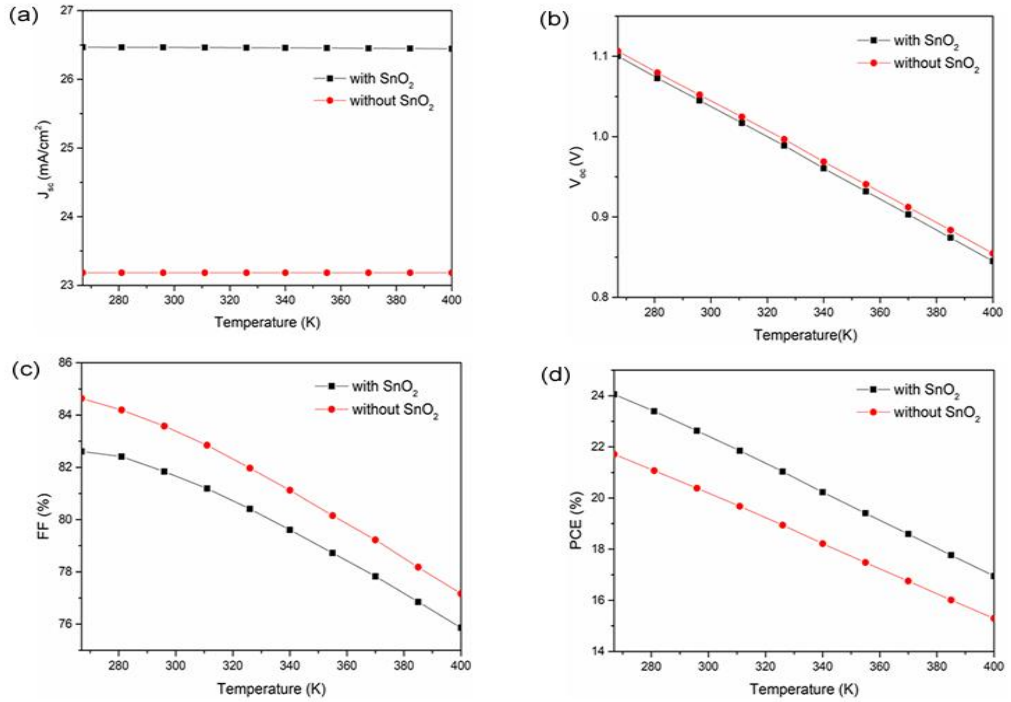

Figure 4. Variation of (a) J_{sc}, (b) V_{oc}, (c) FF and (d) PCE with solar cell working temperature.

Table 3. Effect of temperature on solar cell parameters with and without SnO_2 ETL.

Device structure	Temperature (Kelvin)	V_{oc} (V)	J_{sc} (mA/cm^2)	FF (%)	PCE (%)
With SnO_2	267	1.10	26.47	82.61	24.06
Without SnO_2		1.11	23.18	84.64	21.71
With SnO_2	281	1.07	26.46	82.41	23.40
Without SnO_2		1.08	23.18	84.19	21.07
With SnO_2	296	1.04	26.46	81.84	22.63
Without SnO_2		1.05	23.18	83.58	20.39
With SnO_2	311	1.02	26.46	81.19	21.85
Without SnO_2		1.02	23.18	82.84	19.68
With SnO_2	326	0.99	26.46	80.41	21.04
Without SnO_2		1.00	23.18	81.97	18.94
With SnO_2	340	0.96	26.46	79.61	20.23
Without SnO_2		0.97	23.18	81.12	18.22
With SnO_2	355	0.93	26.45	78.72	19.41
Without SnO_2		0.94	23.18	80.15	17.48
With SnO_2	370	0.90	26.45	77.83	18.59
Without SnO_2		0.91	23.18	79.22	16.75
With SnO_2	385	0.87	26.45	76.85	17.77
Without SnO_2		0.88	23.18	78.18	16.01
With SnO_2	400	0.84	26.44	75.86	16.95
Without SnO_2		0.85	23.18	77.16	15.29

3.3 Effect of Perovskite Absorber Layer Doping Density

Figure 5(a) illustrates the variation of the short-circuit current density (J_{sc}) as a function of donor doping density in the absorber layer. To analyse the effect of perovskite absorber layer, solar cell structure was simulated in the concentration ranging from 10^{10} – 10^{20} /cm^3. **Figure 5(a)** shows that J_{sc} is higher with SnO_2 and it starts to decrease beyond 10^{18}/cm^3. Similar trend was observed for the device without SnO_2 ETL and J_{sc} is low compared to the device with SnO_2.

Figure 5(b) presents the dependence of open-circuit voltage (V_{oc}) on donor doping density for the simulated perovskite solar cell structures. The donor concentration is varied over several orders of magnitude to investigate its influence on the internal electric field, recombination dynamics, and overall solar cell performance. At low donor doping densities (10^{10}-10^{14} cm^{-3}), V_{oc} remains relatively low and nearly constant. In this regime, the weak built-in electric field limits effective charge separation, leading to increased bulk and interfacial recombination. As a consequence, the quasi-Fermi level splitting within the absorber layer is insufficient to produce higher V_{oc} values. As the donor doping density increases to a moderate range (10^{14}-10^{19} cm^{-3}), a noticeable improvement in V_{oc} is observed. This enhancement is primarily attributed to the strengthening of the built-in potential across the junction, which promotes efficient charge separation and suppresses recombination losses. The increased donor concentration improves energy level alignment at the ETL/perovskite interface, resulting in enhanced electron extraction and a higher quasi-Fermi level splitting.

Figure 5(c) presents the dependence of the fill factor (FF) on donor doping density for the simulated perovskite solar cell over a broad doping range (10^{10}-10^{20} /cm^3).

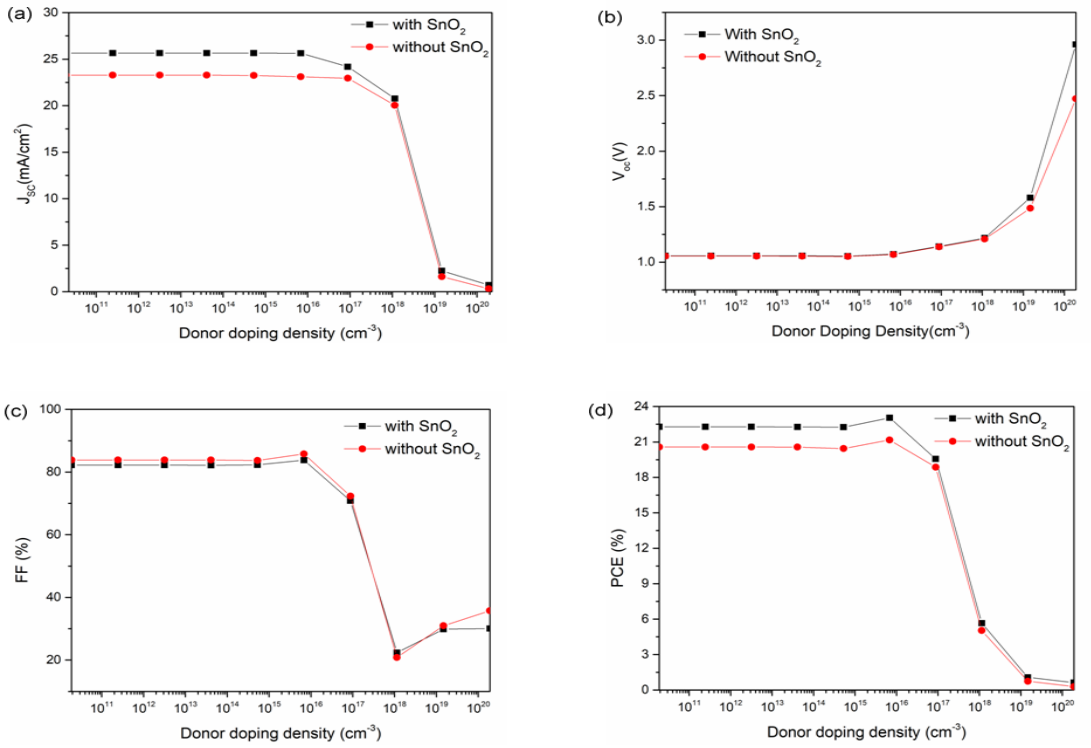

Figure 5. Variation of (a) J_{sc}, (b) V_{oc}, (c) FF and (d) PCE with perovskite layer donor doping density.

Similarly **Figure 5(d)** shows that the effect of variation of donor doping density on PCE. Except Voc, all the parameters such as J_{sc}, FF and PCE start to decrease beyond 10^{16} /cm^3. This shows that photogenerated charge carrier's generation rate does not vary with doping concentration beyond a limit. The data on effect of perovskite layer donor doping density on solar cell output parameters is given in **Table 4**.

Table 4. Effect of perovskite layer donor doping density on solar cell output parameters.

Device structure	Doping density(cm^{-3})	V_{oc} (V)	J_{sc} (mA/cm^2)	FF (%)	PCE (%)
With SnO_2	1.9 x 10^{10}	1.06	25.65	82.22	22.29
Without SnO_2		1.05	23.28	83.85	20.58
With SnO_2	2.45 x 10^{11}	1.06	25.65	82.22	22.29
Without SnO_2		1.05	23.28	83.85	20.58
With SnO_2	3.16 x 10^{12}	1.06	25.65	82.22	22.29
Without SnO_2		1.05	23.28	83.85	20.58
With SnO_2	4.03 x 10^{13}	1.06	25.65	82.17	22.27
Without SnO_2		1.05	23.28	83.85	20.57
With SnO_2	5.29 x 10^{14}	1.05	25.66	82.29	22.26
Without SnO_2		1.05	23.25	83.69	20.45
With SnO_2	6.83 x 10^{15}	1.07	25.64	83.80	23.05
Without SnO_2		1.07	23.11	85.77	21.17
With SnO_2	8.82 x 10^{16}	1.14	24.19	70.86	19.56
Without SnO_2		1.14	22.95	72.31	18.87
With SnO_2	1.14 x 10^{18}	1.22	20.76	22.34	5.65
Without SnO_2		1.21	20.04	20.81	5.04
With SnO_2	1.47 x 10^{19}	1.58	2.26	29.86	1.06
Without SnO_2		1.49	1.61	30.96	0.74
With SnO_2	1.90 x 10^{20}	2.96	0.70	30.05	0.62
Without SnO_2		2.47	0.32	35.74	0.28

3.4 Effect of ETL and HTL Thickness Variation

The variation in ETL and HTL thickness for our simulated structure has been analysed in detail by observing their effect on the device output characteristics. Thickness of ETL and HTL is changed from 50 nm to 500 nm. The effect of ETL and HTL thickness variation on the device output characteristics are shown in **Figure 6**, **Table 5** and **Table 6** respectively.

The ETL and HTL thickness is varied from 50nm to 500nm and it has been observed that there is a slight change in output parameters such as Voc, J_{sc}, FF and PCE. When the ETL is thin J_{sc} drops due to more recombination. If ETL is thick, the Voc and FF decrease due to high series resistance and enhanced charge accumulation and higher recombination at the ETL/absorber interface. On the other hand HTL does not absorb light and only supports to transfer of holes to the electrodes. However, at higher thickness of HTL output parameters decreases due to higher series resistance and limited mobility.

Table 5. Effect of ETL thickness variation on output characteristics.

Thickness(nm)	V_{oc} (V)	J_{sc} (mA/cm^2)	FF (%)	PCE (%)
50	1	25	82.6	20.65
80	1.01	25.67	82.65	21.42
100	1.05	25.66	82.7	22.28
150	1	25.6	82.1	21.01
200	0.95	25.4	82	19.78
250	0.92	25	82	18.86
300	0.91	24.6	81	18.13
350	0.9	24	82	17.71
400	0.89	23.8	82	17.36
500	0.85	23	81	15.83

Table 6. Effect of HTL thickness variation on output characteristics.

Thickness (nm)	V_{oc} (V)	J_{sc} (mA/cm²)	FF (%)	PCE (%)
50	1.04	25.69	82	21.9
80	1.05	25.67	82.5	22.23
100	1.04	25.62	82.5	21.98
150	1.04	25.61	82	21.84
200	1.03	25.6	81.45	21.47
250	1.02	25.55	81.4	21.21
300	1.02	25	80	20.4
350	1.02	24.7	79.8	20.1
400	1.01	24.2	79	19.3
500	1	24	78	18.72

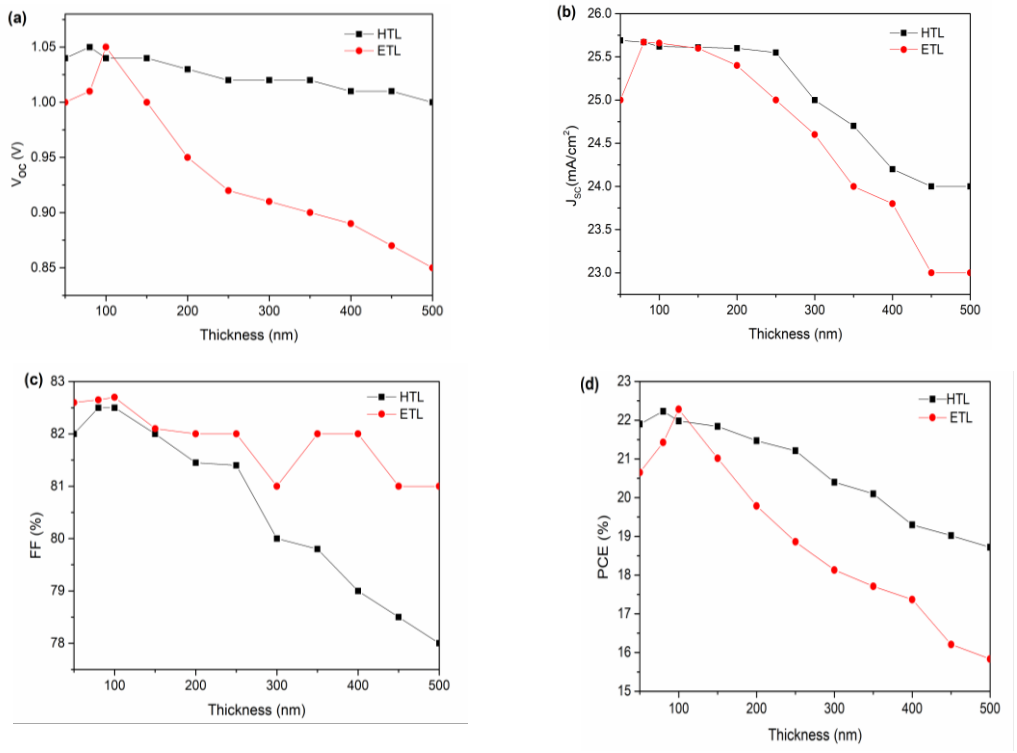

Figure 6. Influence of HTL and ETL thickness on device output characteristics (a) V_{oc} (b) J_{sc} (c) FF (d) PCE.

3.5 Effect of doping in ETL and HTL

We have varied the doping concentration in the device for shallow donor density from 10^{12} to 10^{22} /cm^3 and shallow acceptor density from 10^{10} to 10^{20} /cm^3 to investigate the doping effect of CTL (ETL & HTL) on the performance of perovskite solar cell. **Figure 7** (ETL) and **Figure 8** (HTL) explains the effect of CTL doping on device output parameters. The data on effect of doping in ETL and HTL on output parameters is given in **Table 7** and **Table 8** respectively.

The ETL doping concentration strongly influences the photovoltaic performance of perovskite solar cells. Increasing the doping level enhances ETL conductivity, leading to improved electron extraction and reduced interfacial recombination, which collectively increase the short-circuit current density (J_{sc}), open-

circuit voltage (Voc), and fill factor (FF). These parameters improve progressively with doping and reach optimal values in the range of 10^{18}-10^{19} /cm³, where charge transport is efficient and resistive losses are minimized. Beyond this range, performance gains saturate due to potential over-doping effects, such as increased recombination and transport imbalance. Consequently, the power conversion efficiency peaks at 22.28% near 10^{19} /cm³, identifying ETL doping optimization as a critical strategy for enhancing charge transport and overall device efficiency.

Table 7. Effect of doping in ETL on output parameters.

Shallow donor density[1/cm³]	V_{oc} (V)	J_{sc} (mA/cm²)	FF (%)	PCE (%)
1.00 x 10^{12}	1.05	25.66	82.46	22.21
1.29 x 10^{13}	1.05	25.66	82.62	22.26
1.67 x 10^{14}	1.05	25.66	82.64	22.27
2.15 x 10^{15}	1.05	25.66	82.64	22.27
2.78 x 10^{16}	1.05	25.67	82.64	22.27
3.59 x 10^{17}	1.05	25.67	82.65	22.28
4.64 x 10^{18}	1.05	25.68	82.65	22.28
6.00 x 10^{19}	1.05	25.68	82.65	22.28
7.74 x 10^{20}	1.05	25.68	82.65	22.28
1.00 x 10^{22}	1.05	25.66	82.62	22.25

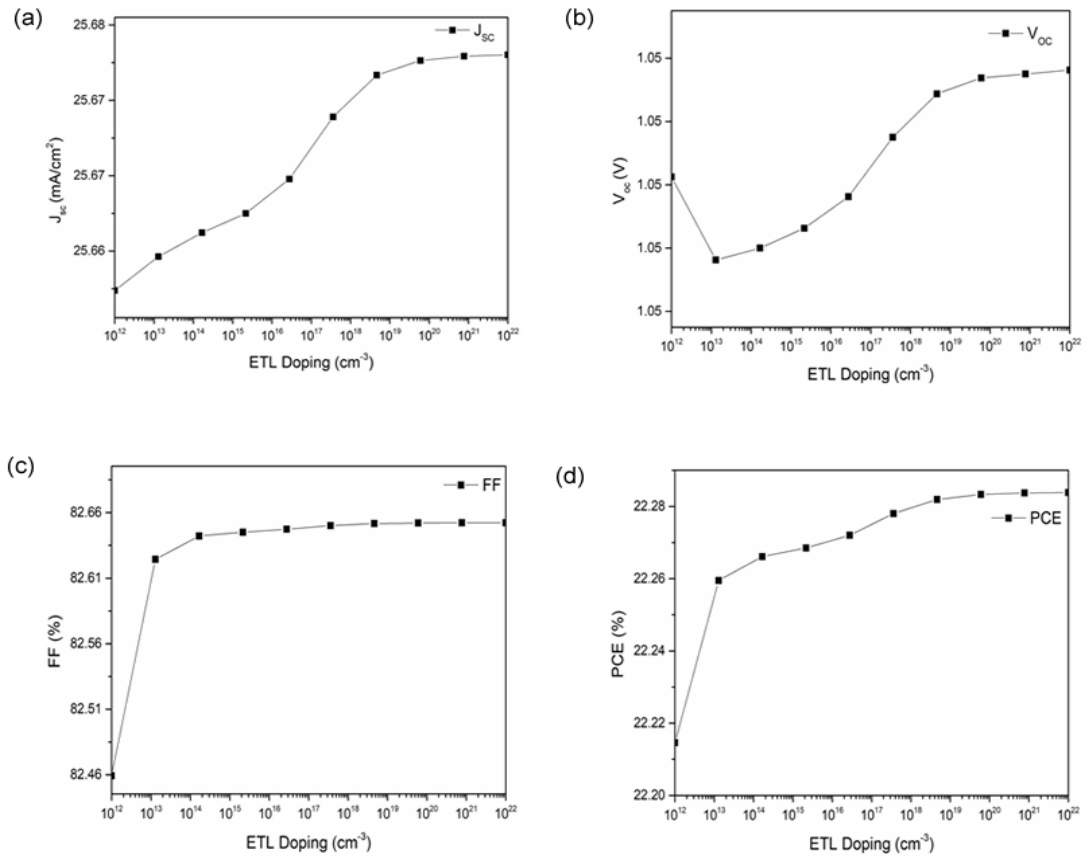

Figure 7. Influence of ETL doping on device output characteristics (a) J_{sc} (b) V_{oc} (c) FF (d) PCE.

Table 8. Effect of doping in HTL on output parameters.

Shallow acceptor density[1/cm³]	V_{oc} (V)	J_{sc} (mA/cm²)	FF (%)	PCE (%)
1.00×10^{10}	1.04	25.66	70.52	18.85
1.29×10^{11}	1.04	25.66	76.04	20.39
1.67×10^{12}	1.05	25.67	80.19	21.56
2.15×10^{13}	1.05	25.67	81.92	22.06
2.78×10^{14}	1.05	25.67	82.52	22.24
3.59×10^{15}	1.05	25.67	82.74	22.31
4.64×10^{16}	1.05	25.67	82.89	22.36
6.00×10^{17}	1.05	25.67	82.94	22.38
7.74×10^{18}	1.05	25.67	82.95	22.39
1.00×10^{20}	1.05	25.65	82.94	22.35

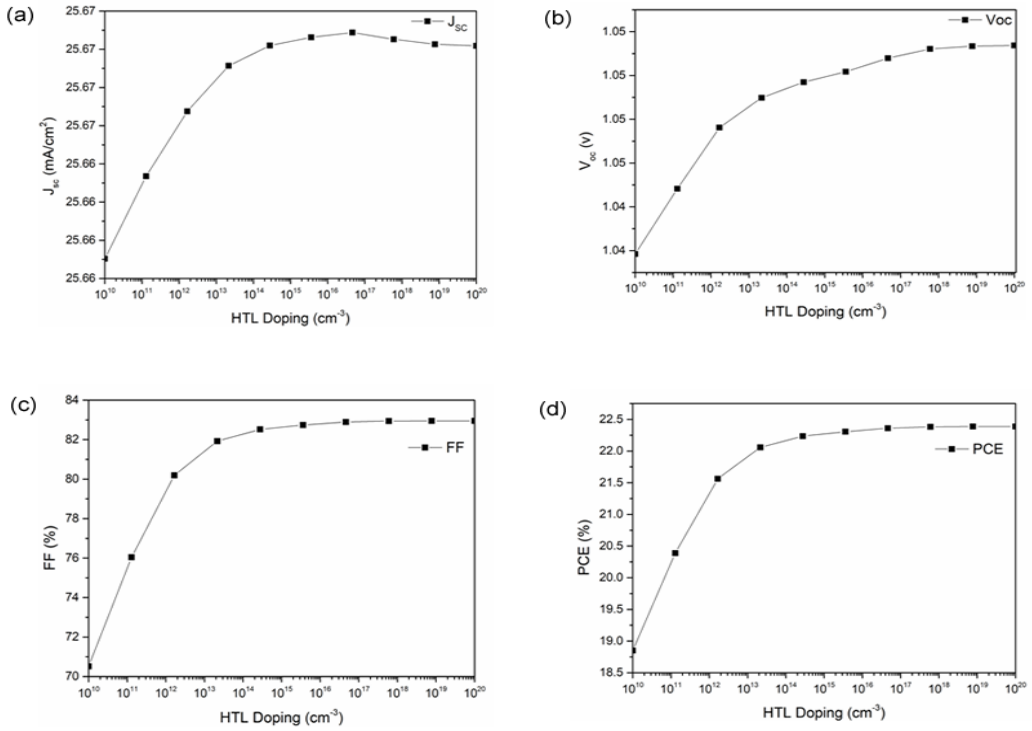

Figure 8. Influence of HTL doping on device output characteristics (a) J_{sc} (b) V_{oc} (c) FF (d) PCE.

The device performance of $FAPbI_3$-based perovskite solar cells exhibits a strong dependence on the hole transport layer doping concentration. Controlled HTL doping enhances hole mobility and interfacial charge extraction, resulting in reduced recombination losses and concurrent improvement in current density, open-circuit voltage, and fill factor. However, excessive doping introduces additional recombination pathways and transport limitations, leading to performance degradation. An optimal doping level of approximately 10^{18} cm^{-3} delivers the highest power conversion efficiency of 22.39%, confirming HTL doping optimization as a critical factor for achieving high-efficiency perovskite devices.

4. Conclusion

This work highlights the effectiveness of SnO_2 as an electron transport layer (ETL) in perovskite solar cells. The integration of SnO_2 provides several key benefits, including high electron mobility, excellent optical transparency, and favourable band alignment with perovskite absorbers. These properties enable efficient charge extraction, reduced recombination losses, and improved solar cell stability compared to conventional ETLs. The simulated device at 267 Kelvin obtained a maximum PCE of 24% and 21.71% with and without SnO_2 ETL respectively. Additionally, the low-temperature processability of SnO_2 makes it suitable for flexible and large-area photovoltaic applications, supporting the scalability of perovskite solar cell technology. Overall, the findings confirm that SnO_2-based ETLs play a pivotal role in enhancing both the performance and durability of perovskite solar cells.

Conflicts of Interest

The authors declare that they have no conflicts of interest.

Acknowledgments

The authors are thankful to Haryana State Council for Science Innovation and Technology (HSCSIT) for providing financial assistance under the R&D research project grant (HSCSIT/R&D/2022/2657 dated 10/10/2022). Authors are thankful to Marc Burgelman, Department of Electronics and Information Systems at the University of Gent, Belgium, for providing SCAPS simulation software. Authors are thankful to University Instrumentation Centre (UIC), Manav Rachna University for research assistance.

AI Disclosure

The author(s) declare that no assistance is taken from generative AI to write this article.

References

Abdelaziz, W., Shaker, A., Abouelatta, M., & Zekry, A. (2019). Possible efficiency boosting of non-fullerene acceptor solar cell using device simulation. *Optical Materials*, *91*, 239-245. https://doi.org/10.1016/j.optmat.2019.03.023

Andreani, L.C., Bozzola, A., Kowalczewski, P., Liscidini, M., & Redorici, L. (2019). Silicon solar cells: toward the efficiency limits. *Advances in physics: X*, *4*(1), 1548305. https://doi.org/10.1080/23746149.2018.1548305

Azadinia, M., Ameri, M., Ghahrizjani, R.T., & Fathollahi, M. (2021). Maximizing the performance of single and multijunction MA and lead-free perovskite solar cell. *Materials Today Energy, 20*, 100647. https://doi.org/10.1016/j.mtener.2021.100647

Bertoluzzi, L., & Bisquert, J. (2017). Investigating the consistency of models for water splitting systems by light and voltage modulated techniques. *The Journal of Physical Chemistry Letters*, *8*(1), 172-180. https://doi.org/10.1021/acs.jpclett.6b02714

Chen, C., Chen, J., Han, H., Chao, L., Hu, J., Niu, T., Dong, H., Yang, S., Xia, Y., Chen, Y., & Huang, W. (2022). Perovskite solar cells based on screen-printed thin films. *Nature*, *612*(7939), 266-271. https://doi.org/10.1038/s41586-022-05346-0

Chen, T., Chen, W.L., Foley, B.J., Lee, J., Ruff, J.P., Ko, J.P., Brown, C.M., Harriger, L.W., Zhang, D., Park, C., Yoon, M., Chang, Y.M., Choi, J.J., & Lee, S.H. (2017). Origin of long lifetime of band-edge charge carriers in organic–inorganic lead iodide perovskites. *Proceedings of the National Academy of Sciences*, *114*(29), 7519-7524. https://doi.org/10.1073/pnas.1704421114

Chen, Y., Li, B., Ye, Y., Zhang, X., Wang, B., Fan, H., Yuliarto, B., Osman, S.M., Yamauchi, Y., & Yin, Y. (2024). Stable FAPbI3 perovskite solar cells via alkylammonium chloride-mediated crystallization control. *ACS Applied Materials & Interfaces*, *16*(22), 28402-28408. https://doi.org/10.1021/acsami.4c01881

Chen, Y., Xu, C., Xiong, J., Zhang, Z., Zhang, X., Yang, J., Xue, X., Yang, D., & Zhang, J. (2018). Benefits of fullerene/SnO2 bilayers as electron transport layer for efficient planar perovskite solar cells. *Organic Electronics*, *58*, 294-300. https://doi.org/10.1016/j.orgel.2018.03.041

ElKhamisy, K., Abdelhamid, H., El-Rabaie, E.S.M., & Abdel-Salam, N., (2024) A comprehensive survey of silicon thin-film solar cell: challenges and novel trends. *Plasmonics, 19*, 1-20. https://doi.org/10.1007/s11468-023-01905-x

Eperon, G.E., Stranks, S.D., Menelaou, C., Johnston, M.B., Herz, L.M., & Snaith, H.J. (2014). Formamidinium lead trihalide: A broadly tunable perovskite for efficient planar heterojunction solar cells. *Energy & Environmental Science, 7*(3), 982-988. https://doi.org/10.1039/c3ee43822h

Fatima, Q., Haidry, A.A., Hussain, R., & Zhang, H. (2023). Device simulation of a thin-layer $CsSnI_3$-based solar cell with enhanced 31.09% efficiency. *Energy & Fuels, 37*(10), 7411-7423. https://doi.org/10.1021/acs.energyfuels.3c00645

Gonzalez, G.S.A., Jeronimo-Rendon, J.J., Wang, Q., Li, G., Alvarez, A.O., Fabregat-Santiago, F., Köbler, H., Alvarado, A., Juárez-Santiesteban, H., Turren-Cruz, S.H., Saliba, M., & Abate, A. (2022). Large grain size with reduced non-radiative recombination in potassium incorporated methylammonium-free perovskite solar cells. *Solar Energy Materials and Solar Cells*, *248*, 111964. https://doi.org/10.1016/j.solmat.2022.111964

Guerrero, A., Bisquert, J., & Garcia-Belmonte, G. (2021). Impedance spectroscopy of metal halide perovskite solar cells from the perspective of equivalent circuits. *Chemical Reviews*, *121*(23), 14430-14484. https://doi.org/10.1021/acs.chemrev.1c00214

Haider, S.Z., Anwar, H., & Wang, M. (2018). A comprehensive device modelling of perovskite solar cell with inorganic copper iodide as hole transport material. *Semiconductor Science and Technology, 33*(3), 035001. https://doi.org/10.1088/1361-6641/aaa596

Han, Q., Bae, S.H., Sun, P., Hsieh, Y.T., Yang, Y., Rim, Y.S., Zhao, H., Chen, Q., Shi, W., Li, G., & Yang, Y. (2016). Single crystal formamidinium lead iodide ($FAPbI_3$): insight into the structural, optical, and electrical properties. *Advanced Materials, 28*(11), 2253-2258. https://doi.org/10.1002/adma.201505002

Hao, F., Stoumpos, C.C., Cao, D.H., Chang, R.P., & Kanatzidis, M.G. (2014). Lead-free solid-state organic–inorganic halide perovskite solar cells. *Nature Photonics*, *8*(6), 489-494. https://doi.org/10.1038/nphoton.2014.82

Hernández-Balaguera, E., & Bisquert, J. (2022). Negative transient spikes in halide perovskites. *ACS Energy Letters*, *7*(8), 2602-2610. https://doi.org/10.1021/acsenergylett.2c01252

Honsberg, C.B., & Bowden, S.G. (2019). Photovoltaics education website. *www.pveducation.org*.

Hosen, R., Sikder, S., Uddin, M.S., Haque, M.M., Mamur, H., & Bhuiyan, M.R.A. (2023). Effect of various layers on improving the photovoltaic efficiency of Al/ZnO/CdS/CdTe/Cu2O/Ni solar cells. *Journal of Alloys and Metallurgical Systems*, *4*, 100041. https://doi.org/10.1016/j.jalmes.2023.100041

Hossain, M.B., Firdous, K.T., Hasan, M.K., Bhuiyan, J.A., Mamur, H., & Bhuiyan, M.R.A. (2025). Enhancing the performance of FAPbI3 using organic and inorganic transport layers in perovskite solar cells. *Total Environment Engineering*, *4*, 100026. https://doi.org/10.1016/j.teengi.2025.100026

Huo, X.N., Wang, K.X., Yin, R., Sun, W.W., Sun, Y.S., Gao, Y.K., You, T.T., & Yin, P.G. (2022). High-performance carbon-based all-inorganic CsPbI2Br perovskite solar cells via ethylammonium iodide and phenethylammonium iodide synergistic passivation. *Solar Energy Materials and Solar Cells*, *247*, 111963. https://doi.org/10.1016/j.solmat.2022.111963

Ishchenko, O., Rogé, V., Lamblin, G., Lenoble, D., & Fechete, I. (2021). TiO_2, ZnO, and SnO_2-based metal oxides for photocatalytic applications: principles and development. *ComptesRendus Chimie, 24*(1), 103-124. https://doi.org/10.5802/crchim.64

Jamal, M.S., Shahahmadi, S.A., Wadi, M.A.A., Chelvanathan, P., Asim, N., Misran, H., Hossain, M.I., Amin, N., Sopain, K., & Akhtaruzzaman, M. (2019). Effect of defect density and energy level mismatch on the performance of perovskite solar cells by numerical simulation. *Optik*, *182*, 1204-1210. https://doi.org/10.1016/j.ijleo.2018.12.163

Jena, A.K., Kulkarni, A., & Miyasaka, T. (2019). Halide perovskite photovoltaics: background, status, and future prospects. *Chemical Reviews*, *119*(5), 3036-3103. https://doi.org/10.1021/acs.chemrev.8b00539

Jiang, Q., Zhang, L., Wang, H., Yang, X., Meng, J., Liu, H., Yin, Z., Wu, J., Zhang, X., & You, J. (2017). Enhanced electron extraction using SnO_2 for high-efficiency planar-structure $HC(NH_2)_2PbI_3$-based perovskite solar cells. *Nature Energy, 2*, Article 16177. https://doi.org/10.1038/nenergy.2016.177

Kanoun, M.B., Kanoun, A.A., Merad, A.E., & Goumri-Said, S. (2021). Device design optimization with interface engineering for highly efficient mixed cations and halides perovskite solar cells. *Results in Physics, 20*, 103707. https://doi.org/10.1016/j.rinp.2020.103707

Kim, H.S., Lee, C.R., Im, J.H., Lee, K.B., Moehl, T., Marchioro, A., Moon, S.J., Humphry-Baker, R., Yum, J.H., Moser, J.E., Grätzel, M., & Park, N.G. (2012). Lead iodide perovskite sensitized all-solid-state submicron thin-film mesoscopic solar cell with efficiency exceeding 9%. *Scientific Reports, 2*(1), 591. https://doi.org/10.1038/srep00591

Kim, H.S., Mora-Seró, I., Gonzalez-Pedro, V., Fabregat-Santiago, F., Juarez-Perez, E.J., Park, N.G., &Bisquert, J. (2013). Mechanism of carrier accumulation in perovskite thin-absorber solar cells. *Nature Communications, 4*(1), 2242. https://doi.org/10.1038/ncomms3242

Kojima, A., Teshima, K., Shirai, Y., & Miyasaka, T. (2009). Organometal halide perovskites as visible-light sensitizers for photovoltaic cells. *Journal of the American Chemical Society, 131*(17), 6050-6051. https://doi.org/10.1021/ja809598r

Liu, F., Ding, C., Zhang, Y., Ripolles, T.S., Kamisaka, T., Toyoda, T., Hayase, S., Minemoto, T., Yoshino, K., Dai, S., Yanagida, M., Noguchi, H., & Shen, Q. (2017). Colloidal synthesis of air-stable alloyed $CsSn_{1-x}Pb_xI_3$ perovskite nanocrystals for use in solar cells. *Journal of the American Chemical Society, 139*, 16708-16719. https://doi.org/10.1021/jacs.7b08628

Mahapatra, A.D., & Lee, J.W. (2022). Metal oxide charge transporting layers for stable high-performance perovskite solar cells. *Crystal Engineering Communications, 24*, 7229-7249. https://doi.org/10.1039/d2ce00825d

Minemoto, T., & Murata, M. (2014). Impact of work function of back contact of perovskite solar cells without hole transport material analysed by device simulation. *Current Applied Physics, 14*(11), 1428-1433. https://doi.org/10.1016/j.cap.2014.08.002

Moyez, S.A., & Roy, S. (2018). Dual-step thermal engineering technique: a new approach for fabrication of efficient $CH_3NH_3PbI_3$-based perovskite solar cell in open air-condition. *Solar Energy Materials and Solar Cells, 185*, 145-152. https://doi.org/10.1016/j.solmat.2018.05.027

National Renewable Energy Laboratory. (2018). *Best research-cell efficiency chart*. https://www.nrel.gov/pv/assets/images/efficiency-chart.png

Noman, M., Shahzaib, M., Jan, S.T., Shah, S.N., & Khan, A.D. (2023). 26.48% efficient and stable $FAPbI_3$ perovskite solar cells employing $SrCu_2O_2$ as hole transport layer. *RSC Advances, 13*(3), 1892-1905. https://doi.org/10.1039/d2ra06535e

Pandey, R., & Chaujar, R. (2017). Technology computer aided design of 29.5% efficient perovskite/interdigitated back contact silicon heterojunction mechanically stacked tandem solar cell for energy-efficient applications. *Journal of Photonics for Energy, 7*(2), 022503. https://doi.org/10.1117/1.JPE.7.022503

Pindado, S., & Cubas, J. (2017). Simple mathematical approach to solar cell/panel behavior based on datasheet information. *Renewable Energy*, *103*, 729-738. https://doi.org/10.1016/j.renene.2016.11.007

Rai, S., Pandey, B., & Dwivedi, D. (2020). Modelling of highly efficient and low-cost $CH_3NH_3Pb(I_{1-x}Cl_x)_3$-based perovskite solar cell by numerical simulation. *Optical Materials, 100*, 10963. https://doi.org/10.1016/j.optmat.2019.109631

Raj, A., Kumar, M., Bherwani, H., Gupta, A., & Anshul, A. (2021). Evidence of improved power conversion efficiency in lead-free $CsGeI_3$-based perovskite solar cell heterostructure via SCAPS simulation. *Journal of Vacuum Science & Technology B, 39*(1), 012401. https://doi.org/10.1116/6.0000718

Ravishankar, S., Aranda, C., Sanchez, S., Bisquert, J., Saliba, M., & Garcia-Belmonte, G. (2019). Perovskite solar cell modeling using light-and voltage-modulated techniques. *The Journal of Physical Chemistry C*, *123*(11), 6444-6449. https://doi.org/10.1021/acs.jpcc.9b01187

Salgado-Conrado, L., Álvarez-Macías, C., & Reyes-Durán, B. (2024). A review of simulation tools for thin-film solar cells. *Materials, 17*(21), 5213. https://doi.org/10.3390/ma17215213

Schulz, P. (2018). Interface design for metal halide perovskite solar cells. *ACS Energy Letters*, *3*(6), 1287-1293. https://doi.org/10.1021/acsenergylett.8b00404

Shockley, W., & Queisser, H.J. (1961). Detailed balance limit of efficiency of p–n junction solar cells. *Journal of Applied Physics, 32*(3), 510-519. https://doi.org/10.1063/1.1736034

Sikder, S., Hosen, R., Uddin, M.S., Haque, M.M., Mamur, H., & Bhuiyan, M.R.A. (2024). Influence of different layers on enhancing the PV performance of Al/ZnO/ZnMnO/CIGSSe/Cu2O/Ni solar cells. *Applied Solar Energy*, *60*(2), 201-214. https://doi.org/10.3103/S0003701X23601357

Son, D.Y., Im, J.H., Kim, H.S., & Park, N.G. (2014). 11% efficient perovskite solar cell based on ZnO nanorods: an effective charge collection system. *The Journal of Physical Chemistry C*, *118*(30), 16567-16573. https://doi.org/10.1021/jp412407j

Tsarev, S., Dubinina, T., Olthof, S., Guererro, A., Luchkin, S.Y., Stevenson, K.J., Aldoshin, S.M., Bisquert, J., Troshin, P.A., & Troshin, P.A. (2023). Stabilizing perovskite solar cells with modified indium oxide electron transport layer. *Solar Energy Materials and Solar Cells*, *251*, 112115. https://doi.org/10.1016/j.solmat.2022.112115

Uddin, M.S., Hosen, R., Sikder, S., Mamur, H., & Bhuiyan, M.R.A. (2024). Photovoltaic performance enhancement of Al/ZnO: Al/i-ZnO/CdS/CIGS/Pt solar cell using SCAPS-1D software. *Next Energy*, *2*, 100080. https://doi.org/10.1016/j.nxener.2023.100080

Wang, D., Wright, M., Elumalai, N.K., & Uddin, A. (2016). Stability of perovskite solar cells. *Solar Energy Materials and Solar Cells*, *147*, 255-275. https://doi.org/10.1016/j.solmat.2015.12.025

Wang, F., & Kumar, S. (2022). Functional thin films for perovskite solar cells. *Coatings*, *12*(7), 952. https://doi.org/10.3390/coatings12070952

Wang, H., Zhang, Z., Wang, X., Duan, L., & Luo, J., (2024). Phenyltrimethylammonium chloride additive for highly efficient and stable FAPbI perovskite solar cells. *Nano Energy, 123*, 109423. https://doi.org/10.1016/j.nanoen.2024.109423

Wang, W., Yang, Z., Ding, J., Kong, J., & Li, X. (2022a). Improving water-resistance of inverted flexible perovskite solar cells via tailoring the top electron-selective layers. *Solar Energy Materials and Solar Cells, 238*, 111609. https://doi.org/10.1016/j.solmat.2022.111609

Wang, Y., Duan, L., Zhang, M., Hameiri, Z., Liu, X., Bai, Y., & Hao, X. (2022b). PTAA as efficient hole transport materials in perovskite solar cells: a review. *Solar RRL, 6*(8), 2200234. https://doi.org/10.1002/solr.202200234

Wozny, S., Yang, M., Nardes, A.M., Mercado, C.C., Ferrere, S., Reese, M.O., Zhou, W., & Zhu, K. (2015). Controlled humidity study on the formation of higher efficiency formamidinium lead triiodide-based solar cells. *Chemistry of Materials*, *27*(13), 4814-4820.https://doi.org/10.1021/acs.chemmater.5b01691

Xia, Z., Meng, J., Chen, C., Wang, H., Zheng, M., Zhou, X., Ding, X., Miao, Y., Zhai, M., & Cheng, M. (2022). Improving the efficiency and stability of perovskite solar cells through tetrabutylammonium hexafluorophosphate post-treatment-assisted top-surface defect passivation. *Solar Energy Materials and Solar Cells, 248*, 112011. https://doi.org/10.1016/j.solmat.2022.112011

Xie, Z., Do, Y., Choi, S.J., Park, H.Y., Kim, H., Kim, J., Song, D., Gokulnath, T., Kim, H.B., Choi, I.W., Jo, Y., Kim, D.S., Yoon, S.Y., Cho, Y.R., & Jin, S.H. (2023). Perovskite solar cells approaching 25% efficiency using side-chain-terminated hole transport materials with low concentration in non-halogenated solvent process. *Journal of Materials Chemistry A*, *11*(17), 9608-9615. https://doi.org/10.1039/D2TA09964K

Xiong, L., Guo, Y., Wen, J., Liu, H., Yang, G., Qin, P., & Fang, G. (2018). Review on the application of SnO_2 in perovskite solar cells. *Advanced Functional Materials, 28*, 1802757. https://doi.org/10.1002/adfm.201802757

Yang, W.S., Park, B.W., Jung, E.H., Jeon, N.J., Kim, Y.C., Lee, D.U., Shin, S.S., Seo, J., Kim, E.K., Noh, J.H., & Seok, S.I. (2017). Iodide management in formamidinium-lead-halide–based perovskite layers for efficient solar cells. *Science, 356*(6345), 1376-1379. https://doi.org/10.1126/science.aan2301

Yin, W.J., Shi, T., & Yan, Y. (2014). Unusual defect physics in $CH_3NH_3PbI_3$ perovskite solar cell absorber. *Applied Physics Letters, 104*(6), 063903. https://doi.org/10.1063/1.4864778

Yoo, J.J., Wieghold, S., Sponseller, M.C., Chua, M.R., Bertram, S.N., Hartono, N.T.P., Tresback, J.S., Hansen, E.C., Correa-Baena, J.P., Bulović, V., Buonassisi, T., Shin, S.S., & Bawendi, M.G. (2019). An interface-stabilized perovskite solar cell with high stabilized efficiency and low voltage loss. *Energy & Environmental Science, 12*(7), 2192–2199. https://doi.org/10.1039/c9ee00751b